

Development of superconductor radiation detectors

Hirohiko M. Shimizu,^{*1} Tokihiro Ikeda,^{*1} Hiroshi Kato,^{*2} Kazuhiko Kawai,^{*1} Hiromasa Miyasaka,^{*2,†1} Takayuki Oku,^{*1} Wataru Ootani,^{*1,†2} Chiko Otani,^{*1} Hiromi Sato,^{*1} Yoshiyuki Takizawa,^{*1} and Hiroshi Watanabe^{*1}

^{*1} Image Information Division, RIKEN

^{*2} Cosmic Radiation Laboratory, RIKEN

Recent results in the development of superconductor radiation detectors using superconducting tunnel junctions applied in the energy measurement of X-rays and the detection of heavy ions are reviewed. The energy resolutions of 41 eV, 58 eV, 65 eV, and 129 eV were obtained for 5.9 keV X-rays with $20 \times 20 \mu\text{m}^2$, $100 \times 100 \mu\text{m}^2$, $200 \times 200 \mu\text{m}^2$, and $500 \times 500 \mu\text{m}^2$ STJs fabricated by introducing a plasma oxidation technique for the suppression of leakage current across the tunneling barrier. The performance in X-ray detection is being improved by the study of phonon-mediated X-ray signals for increasing X-ray detection efficiency and by installing a SQUID signal amplifier for suppression of the signal transmission loss and the electric noise. Direct voltage switching of STJ induced by heavy ions was successfully observed, which opens a new possibility to realize a radiation hard heavy ion detector with the timing characteristics of the order of picosecond.

Introduction

Superconducting tunnel junction (STJ) is a Josephson device comprised of two superconductor layers which are weakly coupled and insulated by a tunneling barrier. Superconducting current carried by Cooper pairs can flow with no voltage difference across the tunneling barrier. Quasiparticles which are uncoupled electrons in superconductor also flow across the barrier according to the quantum mechanical tunneling. The energy deposited in the superconductor layer by an incident radiation generates an excess of quasiparticles and phonons.¹⁾ The amount of the energy deposit can be determined by measuring the total amount of quasiparticles selectively. A magnetic field is usually applied to suppress the superconducting current and the quasiparticle excess is measured after biasing the STJ at a non-zero voltage state. The minimum energy required to excite a quasiparticle is of the order of meV, which is smaller than that required to excite an electron up to the conduction band in semiconductor detectors by three orders of magnitude.²⁻⁶⁾ Therefore, the statistical fluctuation in the total number of the excitation is suppressed by more than one order of magnitude, which results in the improvement of the intrinsic energy resolution. The quasiparticle excess disappears in the time scale of a few microseconds and the STJ comes back to its original state. Therefore, the STJ can be operated at relatively higher temperatures compared with other cryogenic detectors on the basis of the thermal detection, and it is capable of counting individual incident radiation at the rate comparable with semiconductor detectors.⁴⁾

We consider the case when the STJ is current-biased at zero voltage. If the energy deposit is sufficiently large to cause a decrease of the maximum value of Josephson current below the current bias, the STJ is switched to a voltage state irreversibly. A direct switching can be caused on the passage of heavy ions since they deposit a large amount of energy in a thin material. In addition, STJs can survive under a

high radiation dose and only a small change has been observed in the voltage-current curve after accepting a high radiation dose.^{7,8)} Therefore, STJ switching can be applied as a very thin position detector under a high-dose circumstance. A very fast response at the level of picosecond can be expected,⁹⁾ which enables a short flight-path time-of-flight measurement.

In this paper, we review the present status of the development of Nb-based STJs for the energy measurement of X-rays and the detection of heavy ions, together with the fabrication technique and SQUID readout development.

X-ray energy measurement

We fabricated Nb-based STJs with aluminum trapping layers on 3-inch silicon wafers of $400 \mu\text{m}$ thickness. The layer structure is shown in Fig. 1. The aluminum trapping layer was employed for an enhancement of output signal to improve the energy resolution, but it is easily damaged during the photoresist treatment. Therefore, a careful attention was paid in the fabrication of the STJ with aluminum trapping layers for X-ray energy measurement.^{10,11)}

A 50 nm thick Al_2O_3 layer was deposited on the sputter-cleaned silicon substrate. The Al_2O_3 layer was employed to

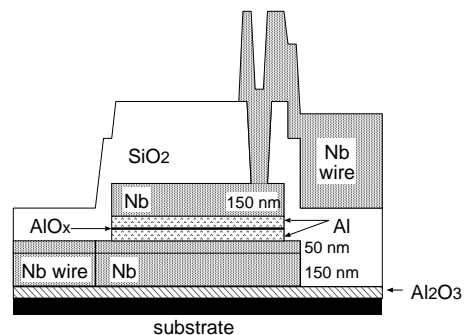


Fig. 1. Cross section of STJ for X-ray detection.

^{†1} Present address: Cyclotron Center, RIKEN

^{†2} Present address: International Center for Elementary Particle Physics, University of Tokyo, 7-3-1 Hongo, Bunkyo, Tokyo 113-0033, Japan

suppress the transmission of energetic phonons induced by X-rays absorbed in the substrate. A 150 nm thick Nb layer was deposited on the Al_2O_3 layer and defined by the reactive ion etching (RIE) after a photolithographic patterning. A multi-layer of Nb(50 nm)/Al(50 nm)/ AlO_x /Al(50 nm)/Nb(150 nm) was deposited on the 150 nm thick Nb layer. The tunneling barrier was formed by a thermal oxidization in a 3990 Pa O_2 atmosphere for one hour. The junctions were structured by RIE and a thin SiO_2 layer was used to avoid the damage on the Al layers during the photoresist treatment as shown in Fig. 2 (a). The surface of junctions were oxidized by a plasma

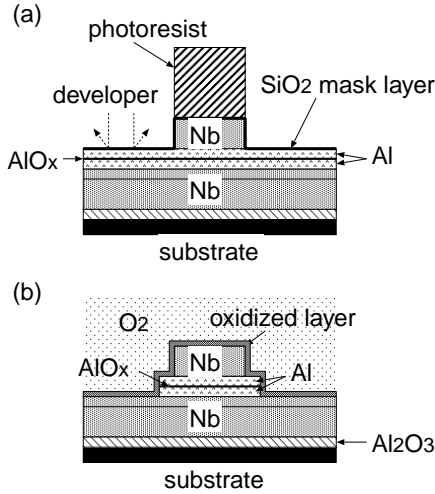


Fig. 2. (a) Schematic view of SiO_2 masking to avoid the damage of Al layer by the developer, (b) Schematic view of oxidization process.

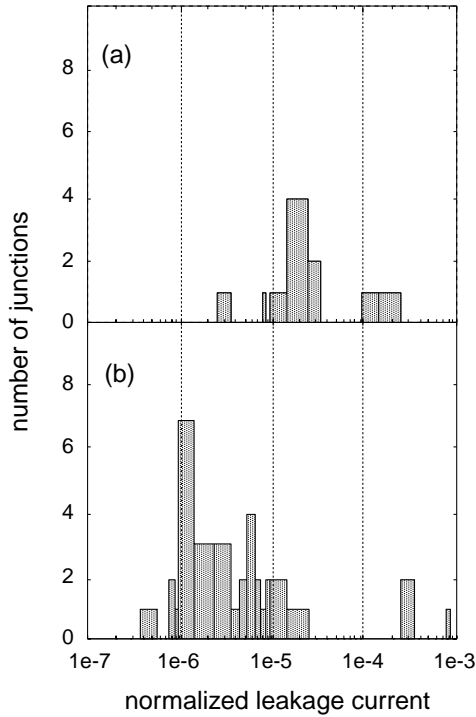


Fig. 3. The distributions of the leakage current at 0.35 K normalized by that at 4.2 K for $100 \times 100 \mu\text{m}^2$ STJs (a) with thermal oxidization (b) with plasma oxidization.

discharge in O_2 atmosphere as shown in Fig. 2 (b). Fabricated STJs were all square shape with the sizes of $20 \times 20 \mu\text{m}^2$, $100 \times 100 \mu\text{m}^2$, $200 \times 200 \mu\text{m}^2$, and $500 \times 500 \mu\text{m}^2$. The critical current density and the normal resistance were $J_c \simeq 130 \text{ A cm}^{-2}$ and $R_N \simeq 90 \text{ m}\Omega$ for $100 \times 100 \mu\text{m}^2$ junctions.

The leakage current at 0.35 K was systematically suppressed compared with the case of a thermal oxidization as shown in Fig. 3.

The STJs were refrigerated at 0.35 K in a depressurized ^3He cryostat and X-rays from a ^{55}Fe radioactive source were introduced to the junctions. The output pulse was amplified using a charge-sensitive preamplifier operated at room temperature. The pulse height of $\sim 600 \text{ mV}$ was obtained with the 2 pF feedback capacitance, which corresponds to a collected charge of 1.2 pC. The preamplifier output was amplified and shaped with the shaping time of $0.5 \mu\text{s}$ and histogrammed using a multi-channel analyzer. Each STJ was biased through a 110 M Ω load resistor connected in series with the STJ placed at room temperature. A constant voltage bias was applied and a nearly constant-current bias was applied to the STJ since the dynamic resistance was much smaller than 110 M Ω .

Obtained pulse height spectra of $100 \times 100 \mu\text{m}^2$ STJs with thermal oxidization and plasma oxidization are shown in Fig. 4 (a) and (b), respectively. Four peaks corresponding

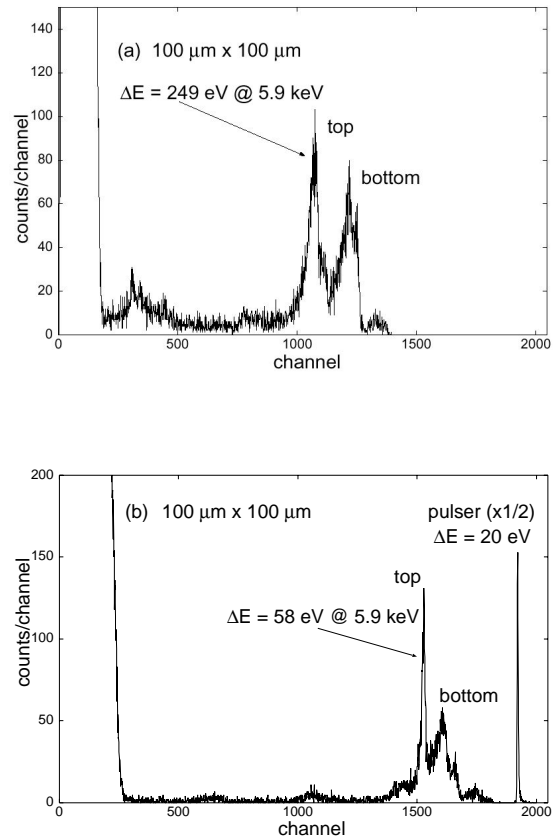


Fig. 4. Pulse height spectra for Mn $K\alpha$ and $K\beta$ from a ^{55}Fe radioactive source. Spectra (a) and (b) were obtained with STJs fabricated with thermal oxidization and plasma oxidization, respectively. In both cases, the junction size was $100 \times 100 \mu\text{m}^2$.

to $K\alpha$ and $K\beta$ X-rays absorbed in top and bottom electrodes were contained in the spectra. Each peak was empirically separated on the plane of pulse height and pulse rise up time.¹⁰⁾ The electrode corresponding to each peak was assigned from the event rate which is approximately proportional to the electrode volume since the electrodes were thin. The base electrode was $120 \times 120 \mu\text{m}^2$ which was $10 \mu\text{m}$ larger on each side than the top electrode. The ratio of event rates corresponding to top and bottom electrodes was 0.52 consistent with the volume ratio of 0.53.

The energy resolution was measured, in the spectra of Fig. 4, to be 249 eV and 58 eV for the peaks corresponding to $K\alpha$ X-rays absorbed in the top electrode. The readout noise was measured from the width of pulser signals and the value of 20 eV was obtained in both cases. The energy resolution was

improved in the case of plasma oxidation according to the suppression of leakage current.

The energy resolution of 41 eV, 65 eV, and 129 eV for 5.9 keV X-rays was obtained with $20 \times 20 \mu\text{m}^2$, $200 \times 200 \mu\text{m}^2$, and $500 \times 500 \mu\text{m}^2$ STJs fabricated with the plasma oxidation as shown in Fig. 5. Corresponding electrodes assigned in the figures were determined assuming the event rate ratio is proportional to the electrode volume ratio. The energy resolution was significantly improved by applying the O_2 plasma oxidation. However, the energy resolution is worse than the limitation of readout noise and intrinsic energy resolution. Fabrication techniques should be improved to suppress the decrease of the signal charge by the quasiparticle recombinations in superconducting layers and at the boundaries of superconducting layers and insulation layers.

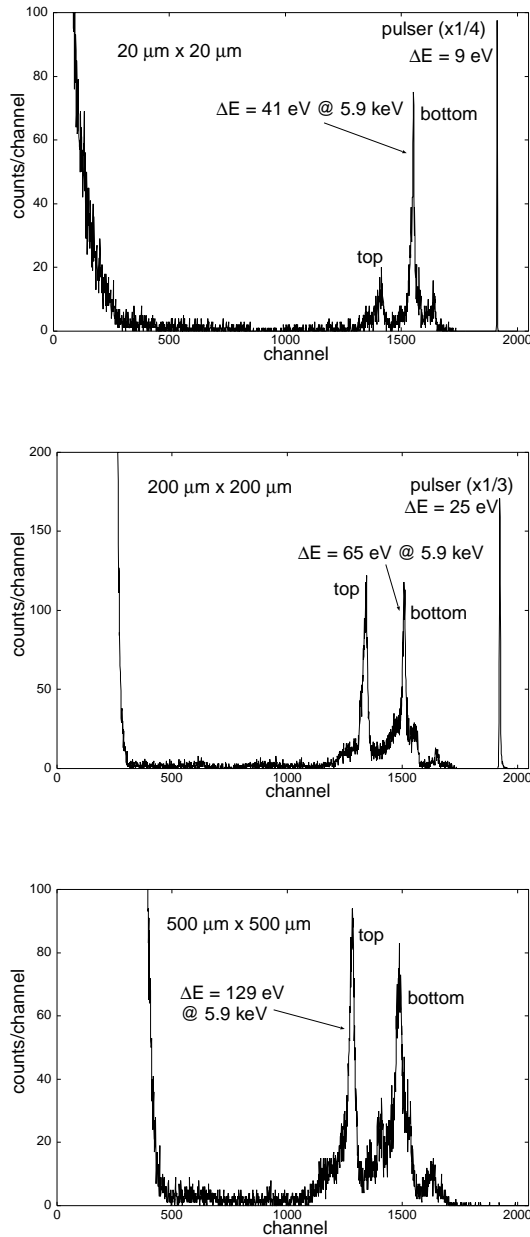


Fig. 5. Pulse height spectra for Mn $K\alpha$ and $K\beta$ from a ^{55}Fe radioactive source obtained with $20 \times 20 \mu\text{m}^2$, $200 \times 200 \mu\text{m}^2$, $500 \times 500 \mu\text{m}^2$ STJs fabricated with plasma oxidation.

Phonon mediated detection of X-rays

The superconducting layers of STJs are not sufficiently thick to realize the detection efficiency close to unity for X-rays in the energy region of a few keV or higher. A large portion of incident X-rays transmits through superconducting layers and absorbed in the substrate and generates energetic phonons, which are observed as a low lying component in the pulse height spectrum.¹²⁾ It also implies that the detection efficiency can be remarkably increased by measuring the quasiparticle excess mediated by energetic phonons generated by X-rays absorbed in the substrate.¹³⁾ We studied the characteristics of the phonon-mediated X-ray signals using Nb-based STJ.¹⁴⁾

STJs were fabricated on a single crystal sapphire substrate of the R-plane orientation without the Al_2O_3 layer. The layer structure was Nb(200 nm)/Al(50 nm)/ AlO_x /Al(25 nm)/Nb(200 nm) and the junctions of $100 \times 100 \mu\text{m}^2$ and $200 \times 200 \mu\text{m}^2$ were used in the experiment. The experimental setup is same as described in the previous section. The obtained pulse height spectra are shown in Fig. 6. In both cases, two peaks at about 1,000 and 1,500 channels correspond to X-rays absorbed in superconducting layers and phonon-mediated signals were observed below ~ 500 channel. The threshold level of the multichannel analyzer was set at ~ 100 channel. The energy resolution was measured to be 181 eV and 219 eV for 5.9 keV X-rays absorbed in the top and bottom electrodes of $100 \times 100 \mu\text{m}^2$ STJ, and 358 eV and 235 eV for $200 \times 200 \mu\text{m}^2$ STJ, respectively.

The spectral shape of the phonon-mediated component was simulated by a Monte-Carlo method assuming that energetic phonons are emitted isotropically from the point where the X-ray is absorbed, and they generate signals if they reach the junction. We introduce a loss of energy transfer across the substrate and the superconducting layer according to the mismatch of the acoustic impedance.¹⁵⁾ We also introduce an adjustable parameter: the radius of the spatially spread phonon cloud generated by X-rays. The simulated spectra are shown with measured spectra in Fig. 7 with the phonon cloud radius of $20 \mu\text{m}$ which reproduced the spectral shape as shown in Fig. 7. It should be noted that the spectral shape was reproduced with single adjustable parameter. The discrepancy between measured and simulated spectra for the

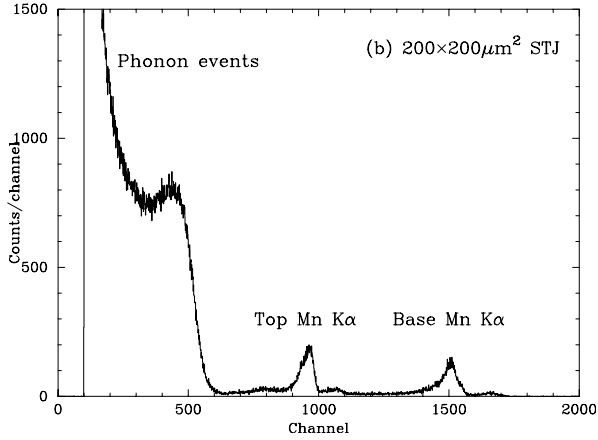
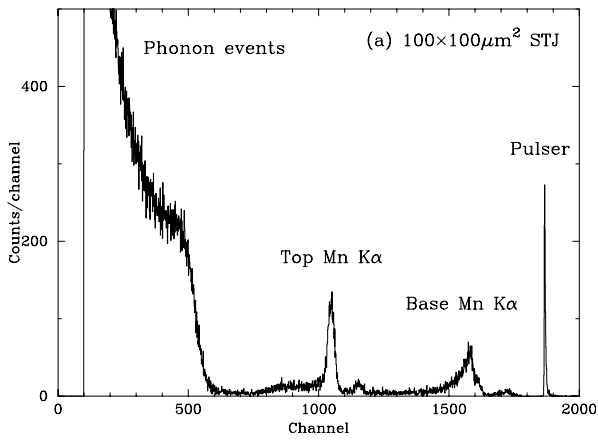


Fig. 6. Pulse height spectra obtained with $100 \times 100 \mu\text{m}^2$ and $200 \times 200 \mu\text{m}^2$ STJs directly fabricated on a sapphire substrate without Al_2O_3 layers.

case of $200 \times 200 \mu\text{m}^2$ STJ may be due to multiple reflection of phonons and the phonon focusing due to the anisotropic phonon propagation in single crystals. More measurements for various energies of incident X-rays would be helpful to improve the simulation model.

SQUID amplifier for X-ray energy measurement

The X-ray signals were transmitted out of the cryostat through co-axial cables in the measurements described above. A current amplifier operated at a cryogenic temperature operated nearby the STJ is desired for (1) realizing constant-voltage bias to stabilize dynamic resistance during the operation (2) transmitting high frequency component to analyze pulse rise up (3) minimizing external electric noise. A low temperature amplifier will be necessary when we develop a large format array of STJ for a large effective area with the imaging capability. SQUID amplifier satisfies the requirements. We developed a SQUID readout system together with a magnetic shield since an external magnetic field is necessary for the energy measurement with STJs but a SQUID amplifier cannot be operated under a magnetic field.^{16,17)}

STJ and SQUID were refrigerated at 0.3K and at liquid helium temperature, respectively, in the cryostat as shown in Fig. 8 (a). The STJ had a layer structure of Nb(200 nm) /

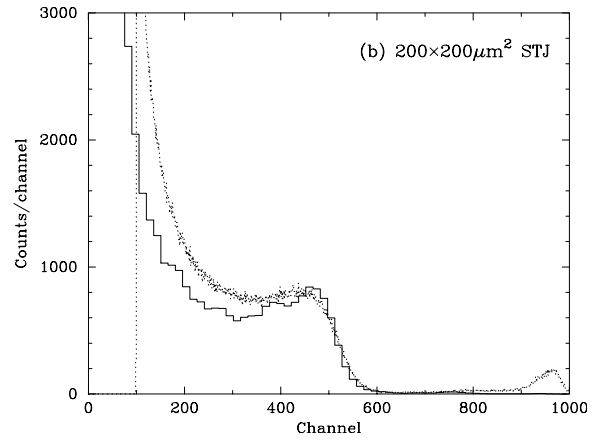
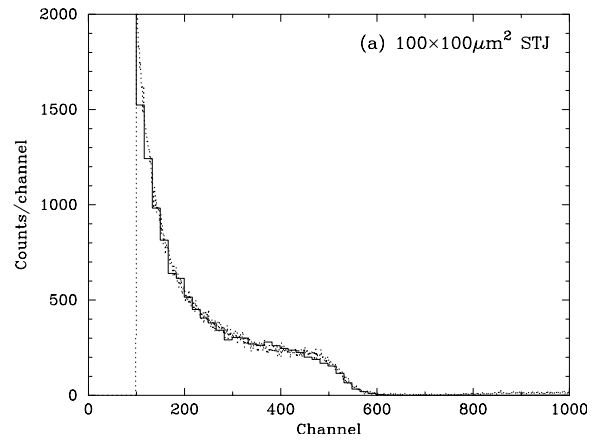


Fig. 7. Comparison of measured spectra (dots) and simulated spectra (solid line). The mismatch of acoustic impedance at the interface between the substrate and the superconducting layer, and the spread of phonon cloud are taken into account. (a) and (b) correspond to $100 \times 100 \mu\text{m}^2$ and $200 \times 200 \mu\text{m}^2$ STJs.

Al(50 nm) / AlO_x / Al(50 nm) / Nb(150 nm). The STJ of $100 \times 100 \mu\text{m}^2$ was used in the measurement and it had the dynamic resistance of $1 \text{ k}\Omega$ and the capacitance of about 400 pF. The SQUID amplifier was two-stage type and had the input inductance of $0.3 \mu\text{H}$. The second stage was comprised of 200 series array SQUID. The SQUID chip was magnetically shielded in a multilayer niobium box in a cryogenic permalloy box. The electric circuit to couple STJ and SQUID is shown in Fig. 8 (b). The capacitance C was chosen to be 100 nF according to a numerical simulation to minimize the pulse deformation. R_s was set to $0.5\text{--}5 \Omega$ to suppress an oscillating component at the signal peak. The signal rise time of $0.3 \mu\text{s}$ was observed with $R_s = 10 \Omega$. The noise level was $3.2 \text{ pA}/\sqrt{\text{Hz}}$ at 1 kHz and $19 \text{ pA}/\sqrt{\text{Hz}}$ at 1 Hz. The SQUID output was amplified by 100 times using an additional amplifier operated at room temperature and sent to a digital oscilloscope. The SQUID amplifier gain was evaluated as $1.8 \times 10^6 \text{ V/A}$.

X-ray signals were histogrammed as a function of total charge calculated from the integration of individual pulse along time. The obtained spectrum for X-rays from a ^{55}Fe radioactive source is shown in Fig. 9. The applied external magnetic field did not give any sizable effect. The energy resolution was 300 eV for the $\text{K}\alpha$ peak in FWHM. The noise level of SQUID amplifier during the measurement was measured to

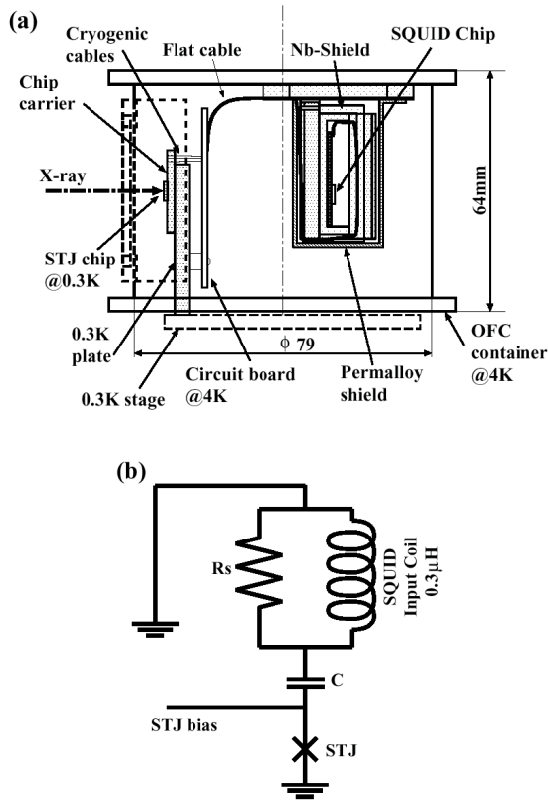


Fig. 8. (a) Configuration of the X-ray detector system, (b) Electrical circuit between an STJ and the SQUID amplifier.

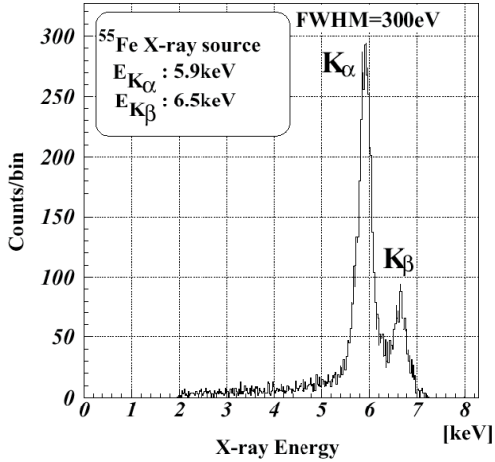


Fig. 9. Energy spectrum for X-ray measured using SQUID amplifier.

be 100 eV, which can be improved by optimizing the parameters of readout circuit and suppressing the electric noise entering through the SQUID bias current.

Heavy ion detection

The STJ-based radiation detector has the radiation hardness and the fast response⁷⁻⁹⁾ together with an excellent energy resolution. A large amount of energy deposited in the STJ causes a decrease of the critical current from I_c down to I_c^* as shown in Fig. 10. If the bias current I_b is applied across the

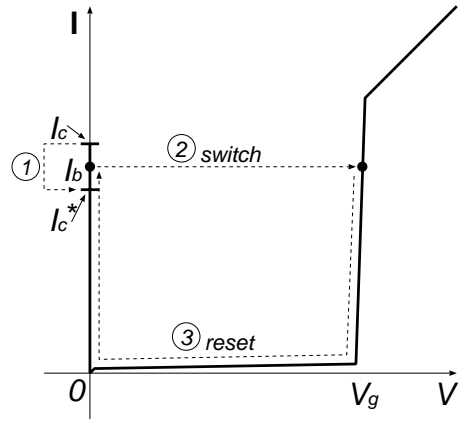


Fig. 10. Schematic view of the detector operation on the basis of the voltage switching, on the I-V curve for an STJ. The critical current is decreased according to an energy deposition in the junction. If the bias is applied at I_b , the voltage across the junction is switched from 0 to V_g . The voltage can be reset by sweeping the bias current to 0 and reset to I_b .

junction, the voltage is switched from 0 to V_g . The voltage switching is irreversible and the voltage is kept at V_g until the bias current is swept down to 0. The switching speed is expected to be of the order of 1–10 ps,⁷⁾ and a very fast timing detection can be realized if the critical current is instantaneously decreased following the passage of the incident radiation.

The decrease of the critical current is explained as the result of the suppression of the superconducting current in a small region where excessive quasiparticles are induced by the incident radiation. The small region is referred to as the hot spot. Heavy ions deposit a large amount of energy on the passage through a matter. Thus, the heavy ions can be detected on the basis of the hot spot mechanism. The STJ-based heavy ion detector enables us to realize a beam profile monitor under a heavy radiation dose and a ps time-of-flight counter.

The irreversible switching has been studied as hybrid superconducting detectors,¹⁸⁻²⁰⁾ which observed the voltage switching induced by electron-hole pairs generated in silicon substrates. We describe the successful observation of instantaneous voltage switching directly induced by heavy ion passage through an STJ.²¹⁾

We used an STJ with the layer structure of Nb(200 nm)/Al(10 nm)-AlO_x/Nb(150 nm) fabricated on a 400 μm thick sapphire substrate. The junction was a square shape and the top Nb layer was 20 × 20 μm² and the bottom Nb layer was 40 × 40 μm². The static properties measured at 4.2 K are listed in Table 1.

We introduced the ⁴⁰Ar beam at 95 MeV/nucleon from

Table 1. STJ properties measured at 4.2 K.

Critical current density	J_c	=	380 A cm ⁻²
Normal resistance	R_N	=	1.5 Ω
Gap voltage	V_g	=	2.9 mV
Quality parameter	V_m	=	75 mV

RIKEN Ring Cyclotron Facility into the STJ immersed in liquid ^4He . The experimental setup and the block diagram of the measurement system are schematically shown in Fig. 11.

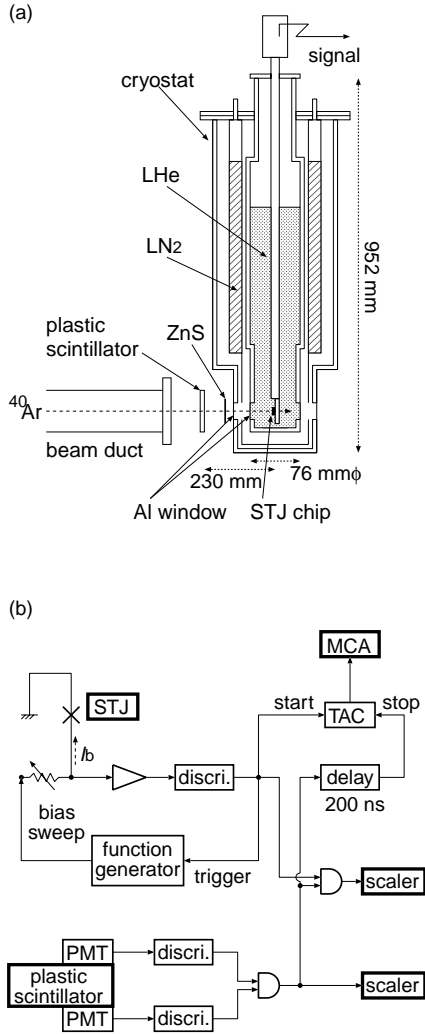


Fig. 11. (a) Experimental setup and (b) the block diagram of data acquisition system.

The time sequence of the measurement is shown in Fig. 12.

Heavy ions went through 0.25 mm thick Al windows attached on the outer vacuum shroud and liquid He bath. A 0.3 mm thick plastic scintillator was placed upstream the cryostat for monitoring the beam intensity. The bias current was supplied using a function generator through a variable resistor. The STJ voltage output V_{out} was amplified and generated a timing pulse in a discriminator. A time-to-analog converter (TAC) was started by the STJ switching signal and stopped by a scintillator signal delayed by 200 ns. The time difference was obtained by histogramming the output pulse height of TAC using a multichannel analyzer. The bias current was reset by sweeping the bias current.

The beam spot size was 10–15 mm in diameter and the entire STJ chip was illuminated. The kinetic energy of ^{40}Ar was degraded down to 44.4 MeV/nucleon on the passage through windows of cryostat and liquid helium. 788 keV was deposited in the STJ and the ^{40}Ar stopped in the liquid He behind the STJ chip.

I_c^* was estimated to be $0.93I_c$ scaling the hot spot size for 5.6 MeV α -particle irradiation.²²⁾ The bias current was set so that $-I_c < I_b < -0.95I_c$.

The trigger rates of the plastic scintillator and the STJ were 400 kHz and 1.1 Hz, consistent with the area ratio. The obtained time spectrum is shown in Fig. 13. The peak was observed in the time spectrum only when the heavy ion beam was incident to STJ and the probability of chance coincidence is negligible. Thus we conclude that the steep peak demonstrates the instantaneous STJ voltage switching induced by heavy ion passage.

The inset of Fig. 13 shows a result of least squares fitting of the peak by two Gaussian functions. The bump at the slower side (negative time) is formed according to a timing fluctuation of the voltage threshold contaminated by electric noise. The time width of the narrower Gaussian was 1.7 ± 0.2 ns in FWHM, which was dominated by the time resolution of the data acquisition system. An improved measurement is being prepared to identify the intrinsic timing characteristics.

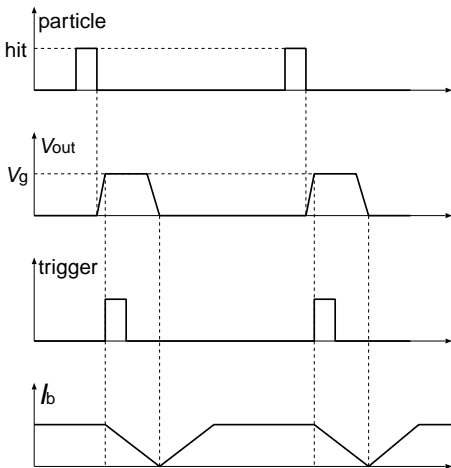


Fig. 12. Timing sequence in the experiment.

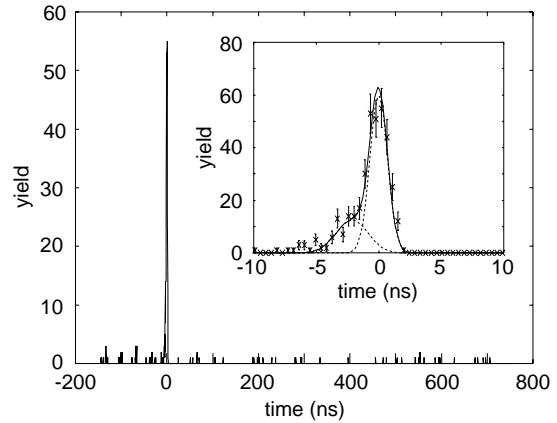


Fig. 13. Time spectrum obtained by histogramming TAC output.

Summary

Superconducting tunnel junctions have potentials to extend the measurement techniques. Fabrication techniques to produce excellent quality STJs with a good reproducibility will be improved for realizing applications in various experiments. The study of the integration technique of STJ and SQUID will introduce flexibilities in applying superconducting radiation detectors.

References

- 1) M. Kurakado: Nucl. Instrum. Methods Phys. Res. **196**, 275 (1982).
- 2) C. A. Mears, S. E. Labov, and A. Barfknecht: Appl. Phys. Lett. **63**, 2961 (1993).
- 3) D. J. Goldie, B. L. Brink, C. Patel, N. E. Booth, and G. L. Salmon: Appl. Phys. Lett. **64**, 3169 (1994).
- 4) C. A. Mears, S. E. Labov, M. Frank, M. A. Lindeman, L. J. Hiller, H. Netel, and A. T. Barfknecht: Nucl. Instrum. Methods Phys. Res. A **370**, 53 (1996).
- 5) M. Frank, C. A. Mears, S. E. Labov, F. Azgui, M. A. Lindeman, L. J. Hiller, H. Netel, and A. Barfknecht: Nucl. Instrum. Methods Phys. Res. A **370**, 41 (1996).
- 6) P. Hettl, G. Angloher, F. V. Feilitzsch, J. Höhne, J. Jochum, H. Kraus, and R. L. Mößbauer: X-Ray Spectrom. **28**, 309 (1999).
- 7) A. Barone and S. De Stefano: Nucl. Instrum. Methods Phys. Res. **202**, 512 (1982).
- 8) S. Pagano et al.: IEEE Trans. Appl. Supercond. **7**, 2917 (1997).
- 9) S. J. Lewandowski et al.: Europhys. Lett. **6**, 425 (1988).
- 10) H. Sato et al.: Inst. Phys. Conf. Ser. No. 167, Vol II, (Proc. Applied Superconductivity, Spain, 14–17, Sep. 1999) p. 683.
- 11) H. Sato et al.: Jpn. J. Appl. Phys. (2000) (in press).
- 12) N. Rando et al.: J. Appl. Phys. **73**, 5098 (1993).
- 13) M. Kurakado, D. Ohsawa, R. Katano, S. Ito, and Y. Isozumi: Rev. Sci. Instrum. **68**, 3685 (1997).
- 14) C. Otani et al.: Jpn. J. Appl. Phys. **39**, 1710 (2000).
- 15) L. M. Brekhovskikh: *Waves in Layered Media* (Academic Press, New York, 1960).
- 16) T. Ikeda et al.: Inst. Phys. Conf. Ser. No. 167, Vol II, (Proc. Applied Superconductivity, Spain, 14–17, Sep. 1999) p. 659.
- 17) T. Oku et al.: Nucl. Instrum. Methods Phys. Res. A **444**, 136 (2000).
- 18) V. Palmieri and A. Esposito: Nucl. Instrum. Methods Phys. Res. A **396**, 277 (1997).
- 19) V. G. Palmieri et al.: Nucl. Instrum. Methods Phys. Res. A **417**, 111 (1998).
- 20) S. Pagano et al.: IEEE Trans. Appl. Supercond. **9**, 3628 (1999).
- 21) H. Sato et al.: Nucl. Instrum. Methods Phys. Res. A (2000), in press.
- 22) R. Cristiano et al.: J. Appl. Phys. **82**, 5024 (1997).